

## Synthesis of Zeolite-Zeolite (MFI-FAU) Composite Catalysts for the Isomerization of *n*-Hexane

<sup>1</sup>Awais Sattar Ghouri\* and <sup>2</sup>Muhammad Rashid Usman

<sup>1</sup>Department of Chemical Engineering, Faculty of Engineering & Architecture, Balochistan University of Information Technology, Engineering & Management Sciences, Balochistan 87100, Pakistan.

<sup>2</sup>Institute of Chemical Engineering & Technology, University of the Punjab, Lahore 54590, Pakistan. ghouriasg@gmail.com\*

(Received on 14<sup>th</sup> October 2016, accepted in revised form 5<sup>th</sup> June 2017)

**Summary:** In this research work, the aim is to produce a relatively novel zeolite-zeolite (MFI-FAU) composite catalyst having better potential of catalyzing isomerization of lighter hydrocarbons such as light naphtha, *n*-pentane, *n*-hexane, *n*-heptane and mixture thereof. A series of zeolite-zeolite (MFI-FAU) composite catalysts have been synthesized by incorporating previous practices and techniques. The catalytic performance of as-synthesized zeolite-zeolite (MFI-FAU) composite catalysts have been investigated by isomerizing 95% pure *n*-hexane in conventional fixed bed flow micro-reactor at temperature 200-240 °C under atmospheric pressure. In order to explore chemical and physical features of zeolite-zeolite (MFI-FAU) composite catalysts, they are examined and characterized using powder X-ray diffraction (XRD), scanning electron microscopy (SEM) coupled with energy-dispersive X-ray spectrometry (EDX), N<sub>2</sub> adsorption-desorption measurements (BET, BJH, t-plot measurements) and Fourier transform infrared (FTIR) spectroscopy equipped with attenuated total reflectance (ATR) arrangements.

**Keywords:** Isomerization, Composite Catalysts, *n*-hexane, Y- Zeolite, ZSM-5.

### Introduction

The valuable products particularly, liquefied petroleum gas (LPG), naphtha, kerosene, diesel, and gas oil coming out of the distillation unit are required to be further treated to yield useful and better hydrocarbon products by using processes such as cracking, isomerization, reforming, etc. These processes alter the inherent characteristics of hydrocarbons into better hydrocarbon fractions by modifying their chemical structure and composition [1]. For instance, straight run naphtha is a mixture of hydrocarbons containing 5 to 10 carbon atoms. It is mostly comprised of straight chain hydrocarbons and has very limited applicability due to low octane number [2]. Therefore, it has to be modified into branched hydrocarbons for better utilization from the point of view of fuel and as good feedstock for making more useful chemical products.

In this connection, isomerization (also known as rearrangement process) is the process in which one isomer is transformed to another isomer having identical composition and molecular weight but different geometrical arrangement of molecules. The number of atoms in any isomer is same but arrangement of atoms is different, which in turn alters the chemical and physical properties to a great extent.

In the light of the stringent environmental laws, isomerization is a good process as it enhances the octane number of hydrocarbons especially lighter

hydrocarbon in the range of C<sub>5</sub>-C<sub>6</sub> by converting their straight-chain structure into branched chain structure without producing aromatics in the products [3]. The ecological properties of branched chain hydrocarbons are far better and efficient than straight chain hydrocarbons, e.g., high octane number petrol burns efficiently causing less damage to engine and environment. Furthermore, fuels blended with branched chain hydrocarbons have clean and green emissions. In view of the acute environmental protection awareness and imposed strict regulations regarding minimizing benzene, sulfur, aromatic and lead contents in fuels, the global petroleum industry is concerned with marketing of clean and safe fuels which must be free from the above mentioned contaminants. Moreover, utilization of straight chain hydrocarbons makes fuel unsuitable for burning purposes, therefore it is impossible to run them in gasoline pool. In this regard, isomerization is recognized as a best process which is indeed playing a pivotal role in conversion of low octane normal paraffins (especially C<sub>5</sub>-C<sub>6</sub>) to their corresponding branched isomers [1].

Catalysts are capable of not only accelerating a chemical reaction but also improve the selectivity of desired products by suppressing the unwanted side reactions. A great variety of modification options are available in changing the shape, structure and size of catalyst which in turn modifies the inherent

---

\*To whom all correspondence should be addressed.

characteristic of catalyst to a great extent. Each modified catalyst design has its own unique characteristic and application in catalysis which is different from other catalyst. Catalyst play key role in producing selective components and make this possible to precede reactions at much mild temperature and pressure conditions which otherwise take place at very high temperature and pressure values. Moreover, catalyst assists in carrying out particular reaction in a much better and controlled manner thereby ensuring safety for working personnel and process equipment. Hence researchable options are enormous in designing new better catalyst for particular reaction mechanism [1].

An important class of alumino-silicate catalyst is zeolite and has attracted attention in catalysis. Zeolites have been the focus of researchers, oil refineries, and environmental protection agencies as they have the ability to catalyze many important chemical reactions such as alkylation, isomerization, cracking, petrochemical catalytic reactions, and green environmental friendly reactions at much controlled and better rates and at optimum reaction conditions [4]. Furthermore, zeolites are regarded as versatile catalysts because of their following dynamic features:

- High hydrothermal and thermal stability
- High surface area
- High catalytic activity
- Multidimensional ordered porous structure
- Strong Bronsted and Lewis acid sites
- Shape selectivity

For selectivity and conversion of desired product, composite catalysts play a vital role in catalyzing much industrial reaction in a much better way with sound synergic effects. It is known that sometimes there arise similarities between guest molecules of reaction mixture and micropore diameter of zeolites, which in turn slows down the reaction rate on behalf of diffusional limitations. Molecular transport can be made easy by carefully connecting macropores or mesopores with zeolite micropore structure. Although mesoporous materials offer quite high external surface area, large volume and channel structure but their practical applications were hit with setback by their inefficient hydrothermal stability, weak acidic sites, and amorphous pore wall. Due to aforementioned limitations of single zeolitic material, continuous efforts have been made by numerous research groups to bring forward the practical knowledge and applications of zeolite-zeolite composite catalysts. The combined effect of different properties of

zeolite-zeolite composite catalysts enhances the catalytic performance due to formation of healthy active sites for catalysis, good hydrothermal stability and much better synergic effect as reported in various research works [5]. Listed below are some of the practical applications of zeolite-zeolite composite catalyst:

- a) Passivating external surface acidic sites of HZSM-5 with non-acidic silicate membrane enhances the selectivity of *p*-xylenes in toluene disproportionation [6].
- b) Blanketing SBA-15 with structured core-shell composite USY improves the selectivities in the range of C<sub>2</sub>-C<sub>5</sub> in *n*-hexadecane cracking [7].
- c) NiW- supported zeolite catalyst promotes the hydrocracking of heavy oil in a much better and controlled manner.
- d) Composite catalyst of Y and  $\beta$ -zeolite shows good catalytic performance and longer life when experimentally investigated for catalytic reduction of nitric oxide in presence of methane and excess O<sub>2</sub> [8].

At the present, no significant research work has been reported related to isomerization of lighter hydrocarbon (especially *n*-hexane, *n*-heptane, *n*-octane, light naphtha, etc.) using zeolite-zeolite composite catalyst. On the other hand, enormous amount of research work has been dedicated to metal impregnated catalysts, which showed positive result for the isomerization process but is considered as costly process due to loading of relatively noble and rare earth metals such as Pt, Pd, Rh, La, Ce, etc. on catalyst surface.

As far this research work is concerned, the aim is to design a relatively novel zeolite-zeolite (MFI-FAU) composite catalysts having better potential of catalyzing isomerization of lighter hydrocarbons such as light naphtha, *n*-pentane, *n*-hexane, *n*-heptane and mixture thereof. The catalytic performance of zeolite-zeolite (MFI-FAU) composite catalysts have been investigated by isomerizing 95% pure *n*-hexane in conventional fixed bed flow micro-reactor at temperature 200-240 °C under atmospheric pressure. It was well noted that the blended properties of both ZSM-5 and Y-zeolite was far better than individual properties of HSM-5 and Y-zeolite, as they have shown better yield of the branched hydrocarbons. In order to explore chemical and physical features of zeolite-zeolite (MFI-FAU) composite catalysts, they are characterized using different techniques.

## Experimental

### Materials

The detailed specifications of chemicals used for synthesizing zeolite-zeolite (MFI-FAU) composite catalyst are depicted in Table-1. No further purification of the chemicals was done. Double distilled water (H<sub>2</sub>O) was obtained by using Direct-Q distilled water machine.

Table-1: CAS numbers, purities, and suppliers of materials used.

Chemical Name	CAS No.	Purity %	Supplier
Sodium Hydroxide (NaOH)	1310-73-2	> 98 %	MERCK
Tetra Propyl Ammonium Bromide (TPABr)	1941-30-6	98 %	SIGMA-ALDRICH
Aluminum Isopropoxide (C <sub>9</sub> H <sub>21</sub> AlO <sub>3</sub> )	555-31-7	≥ 99.99 %	SIGMA-ALDRICH
Fumed Silica (SiO <sub>2</sub> ) (0.2-0.3µm)	112945-52-5	99.8 %	SIGMA-ALDRICH
Ammonium Chloride (NH <sub>4</sub> Cl)	12125-02-9	≥ 99.8 %	MERCK

### Material Synthesis

Previously reported procedures and practices were utilized for synthesizing zeolite-zeolite (MFI-FAU) composite catalysts [9]. In the first step, 0.22 g of sodium hydroxide (NaOH) was dissolved in 36 ml of double distilled water. 3.02 g of tetra propyl ammonium bromide (TPABr) was then added as templating agent in NaOH solution with continuous stirring. Then the mixture was stirred for 30 min. After that 3.85 g of fumed silica was added to solution of NaOH and TPABr with continuous stirring. The whole mixture was then uniformly stirred for 1h.

In the second step, 1.09 g of sodium hydroxide (NaOH) was dissolved in 26 ml of double distilled water. 0.42 g of aluminum isopropoxide (C<sub>9</sub>H<sub>21</sub>AlO<sub>3</sub>) and 72 ml of double distilled water as solvent was then added to NaOH solution with continuous stirring. Then the mixture was stirred for 45 min. After that 2.98 g of fumed silica was added to solution of NaOH and C<sub>9</sub>H<sub>21</sub>AlO<sub>3</sub> with continuous stirring. The whole mixture was then uniformly stirred for 1 h.

Finally, the seeding gel prepared in step 1 was slowly added to seeding gel prepared in step 2 with continuous stirring. The whole mixture was gently stirred for 1 h to obtain homogenized mixture with a pH of 11.3. Then, 3.41 g of aluminum isopropoxide and 2 g of Y-zeolite (CBV100, nominal SiO<sub>2</sub>/Al<sub>2</sub>O<sub>3</sub> = 5.1. Na-form) were added to the mixture. The new mixture obtained was then uniformly stirred for 1 h at room temperature and

then transferred into Teflon lined autoclave. The contents of the autoclave were heated to 110 °C for 48 h. The final solid product obtained was filtered and washed with plenty of double distilled water and dried at room temperature for 1 day and then dried in vacuum oven at 110 °C for 6 h. The sodium form of catalyst was finally treated with 1M ammonium chloride (NH<sub>4</sub>Cl) solution to obtain NH<sub>4</sub><sup>+</sup> form, which was then subsequently transformed into H-form catalyst by calcining in furnace at 500 °C for 6h. Two similar catalysts were prepared by varying Y-zeolite amount (3 g and 4 g) through the aforementioned procedure. The three catalysts were named A, B, and C.

### Characterization

The textural properties of the synthesized Zeolite-Zeolite (MFI-FAU) composite catalysts such as surface area, micropore area, pore volume, micropore volume and pore size were measured by using N<sub>2</sub> adsorption-desorption isotherm at -196.15 °C using Micromeritics (ASAP 2020) surface area and porosity analyzer. Prior to N<sub>2</sub> physisorption, a known quantity of catalyst sample was degassed at 219.85 °C under vacuum (10-5 Torr) for 3 h. The specific surface area was calculated using Brunauer, Emmet, and Teller (BET) and Langmuir equations. Micropore area, micropore volume and external surface area were analyzed using t-plot method and pore size distribution was determined using Barrett, Joyner, and Halenda (BJH) method.

Crystallinity of the prepared catalysts were inspected in the form of XRD patterns by using PANalytical X'Pert<sup>3</sup> Powder (Almelo, Netherlands) diffractometer, which used Beta-filtered Cu K $\alpha$  radiation ( $\lambda = 0.1540$  nm) with incident beam path of 240 mm and was operated at 45 kV and 40 mA with a scanning range of  $2\theta$  from 5° to 50° at a scanning rate of 2° min<sup>-1</sup>.

The crystal size and surface morphology of the catalysts were investigated on MIRA3 TESCAN (Brno, Czech Republic) scanning electron microscopy (SEM) equipped with Energy Dispersive X-Ray Spectrometry (EDX).

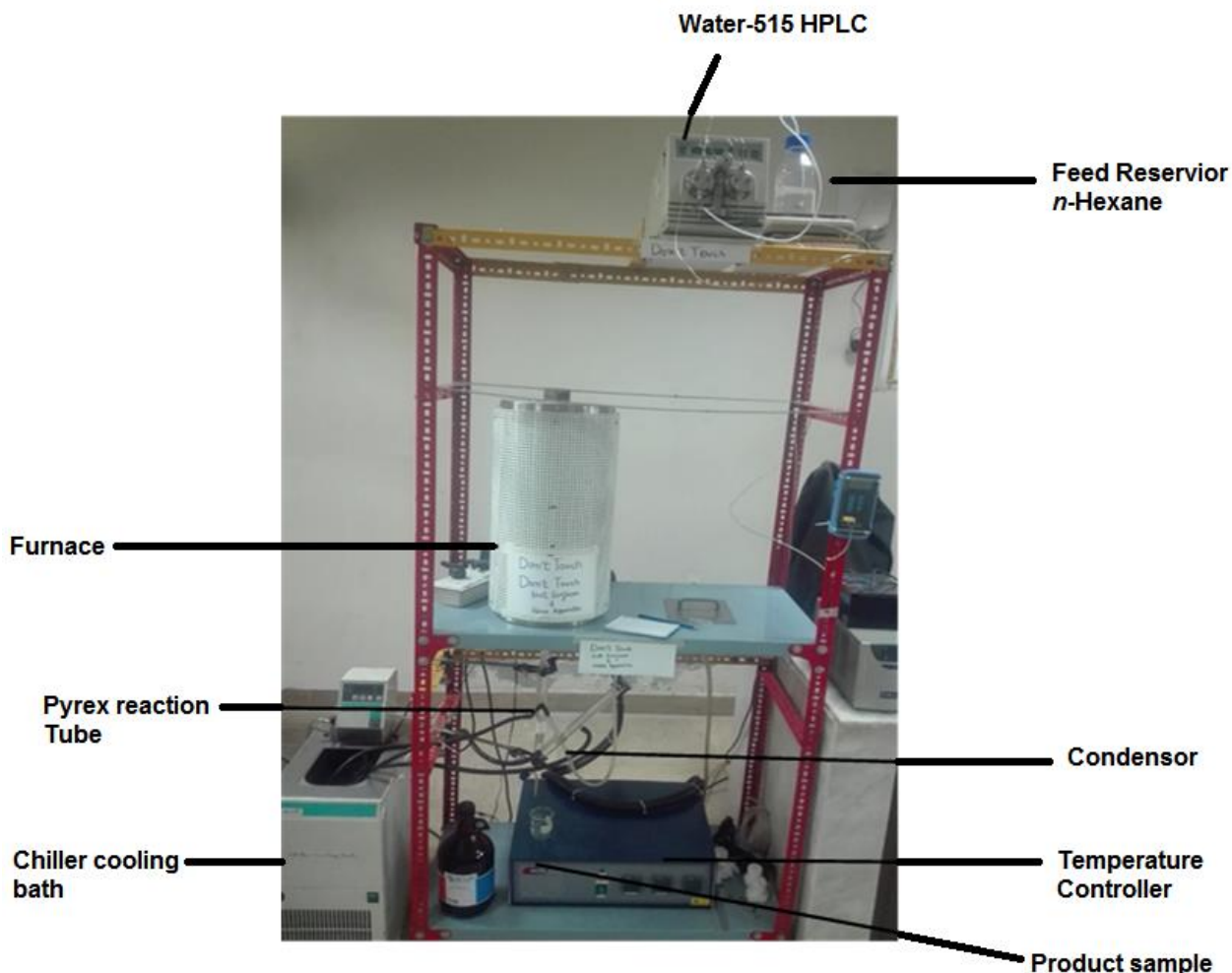
Fourier Transform Infrared (FT-IR) analysis of the prepared catalysts were performed with a Shimadzu IRPrestige-21 equipment coupled with attenuated total reflectance (ATR) arrangements using KBr discs, in the range of 400–4000 cm<sup>-1</sup>.

The catalytic activity of the zeolite-zeolite (MFI-FAU) composite catalysts were examined by isomerizing *n*-hexane in conventional fixed bed flow

micro-reactor apparatus with a pyrex tube (i.d. of 12.7 mm) under atmospheric pressure at 200-240 °C with weight hourly space velocity (WHSV) of 0.25-0.06 g. h<sup>-1</sup>/g-catalyst, where W is the weight of catalyst in g and F<sub>A<sub>0</sub></sub> is the feed rate in g.h<sup>-1</sup>. The general specification of *n*-hexane (reactant) and the experimental set-up used for *n*-hexane isomerization is shown in Table-2 and Fig. 1, respectively. For each experimental run, prior to loading of catalysts in reactor alongwith glass beads (3 mm) and quartz wool, 1 g catalyst was pelletized and sieved in the range of 710-425 μm. The *n*-hexane was fed by Waters-515 HPLC pump (without any carrier gas) at different flowrate in the range of 0.1-0.4 ml/min. An off-line gas chromatograph (GC-2014, Shimadzu) equipped with TRB-1 capillary column (0.25 mm ID × 100 m: Teknokroma) and FID detector were used to analyze, identify, and quantify the hydrocarbon components in *n*-hexane and the hydrocarbon products of the reaction.

Table-2: Specifications of *n*-hexane (Reactant).

General Description about Reactant	
Name of Reactant	<i>n</i> -hexane
Purity of Reactant	95 %
Grade of Reactant	Analytical Grade
Manufacturer of Reactant	Lab-Scan (Thailand)
Assay (GC)	95 %
Formula Weight (F.W)	86.18
Boiling Point (B.P)	68.7 °C
$n_D^{20}$	1.374
$d_{20}^{20}$	0.659
Maximum Impurity Level in <i>n</i> -hexane	
Water (H <sub>2</sub> O)	0.02 %
Acidity (mEq./g)	0.0005 %
Evaporation Residue	0.001 %
Sulfur Compounds	0.001 %
Organic Residue (as Toluene by GC/FID)	Max. 10 ng/ml
Halogenated Residues (as Lindane by GC/FID)	Max. 10 ng/ml
Trichloromethane	< 1 ppb

Fig. 1: Experimental set-up used for the isomerization of *n*-hexane.

## Results and Discussion

Fig. 2 shows the XRD pattern of as-synthesized zeolite-zeolite (MFI-FAU) composite catalysts. As depicted from Fig. 2 that peaks at  $6.16^\circ$ ,  $10.08^\circ$ ,  $19.01^\circ$ ,  $20.24^\circ$ ,  $24.24^\circ$ ,  $27.24^\circ$ , and  $32.00^\circ$  are the characteristic peaks of FAU zeolite phase [10-12] which exactly corresponds to the typical peaks of Y-zeolite as indexed in Joint Committee on Powder Diffraction Standards (JCPDS) data with reference code 39-1380 [16]. Similarly, peaks at  $15.8^\circ$ ,  $23.00^\circ$ ,  $28.23^\circ$ , and  $30.03^\circ$  are the characteristic peaks of MFI zeolite phase [12, 17, 18] which exactly correspond to the typical peaks of ZSM-5 as indexed in Joint Committee on Powder Diffraction Standards (JCPDS) data with reference code 00-037-0359 [16]. Above mentioned results are observed in all prepared zeolite-zeolite (MFI-FAU) composite catalysts which clarify the co-existence of Y and ZSM-5 zeolite phase in synthesized composite catalysts.

Chemical composition of zeolite can better explain its properties [19]. The SEM images as shown in Fig. 3-5 confirm the presence of respective flower-like and block-like crystalline particles of Y and ZSM-5 zeolite in the as-synthesized zeolite-zeolite (MFI-FAU) composite catalysts. The EDX results as can be

seen from Fig. 6-8 and Table-3 shows that Si/Al ratio in the synthesized composite catalysts, i.e. Catalyst-A, Catalyst-B, and Catalyst-C were found to be 6.6, 6.3, and 4.7 on weight % basis and 6.4, 6.0, and 4.6 on atomic % basis respectively.

Table-3: The results obtained from EDX analysis of the Catalyst samples.

Catalyst-A				
Element	Weight %		Atomic %	
Si K	86.9		86.5	
Al K	13.1	Si/Al = 6.6	13.5	Si/Al = 6.4
Total	100		100	
Catalyst-B				
Element	Weight %		Atomic %	
Si K	86.3		85.8	
Al K	13.7	Si/Al = 6.3	14.2	Si/Al = 6.0
Total	100		100	
Catalyst-C				
Element	Weight %		Atomic %	
Si K	82.6		82	
Al K	17.4	Si/Al = 4.7	18	Si/Al = 4.6
Total	100		100	

The above mentioned results strongly confirm that silicon species out of ZSM-5 zeolite have transferred to Y-zeolite structure. This transformation of silicon indicates that our target zeolite-zeolite (MFI-FAU) composite catalysts have successfully been formed. It has also been deduced from EDX results that Si/Al ratio has been reduced (as discussed above) in as-synthesized zeolite-zeolite (MFI-FAU) composite catalysts.

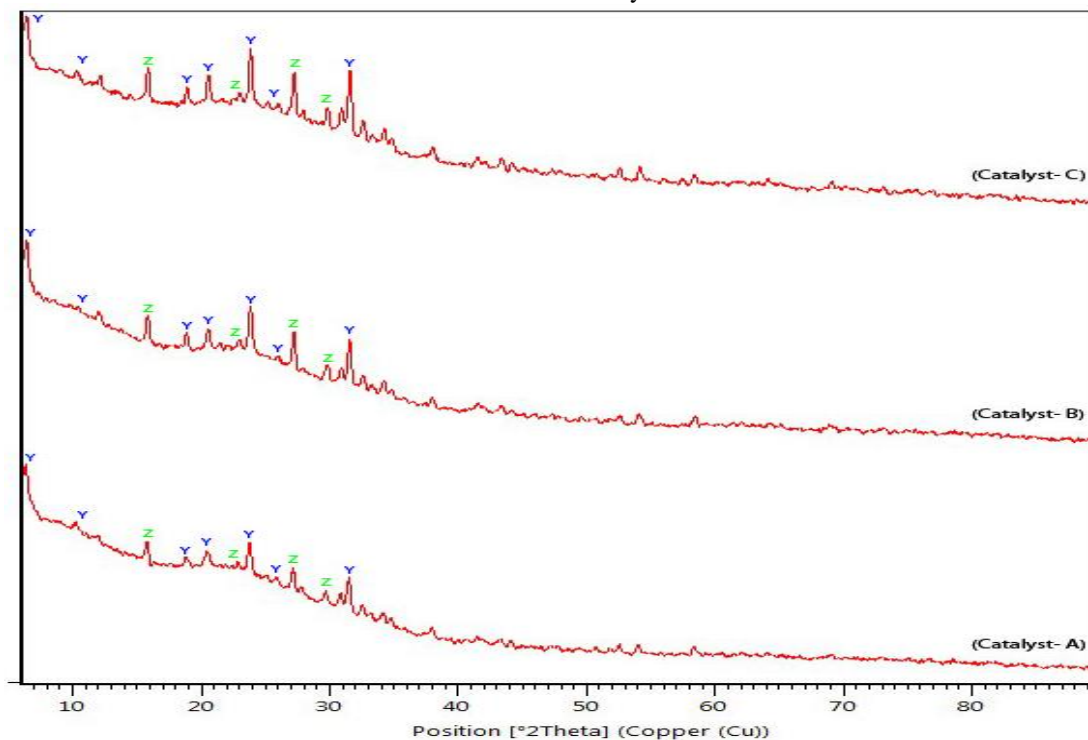
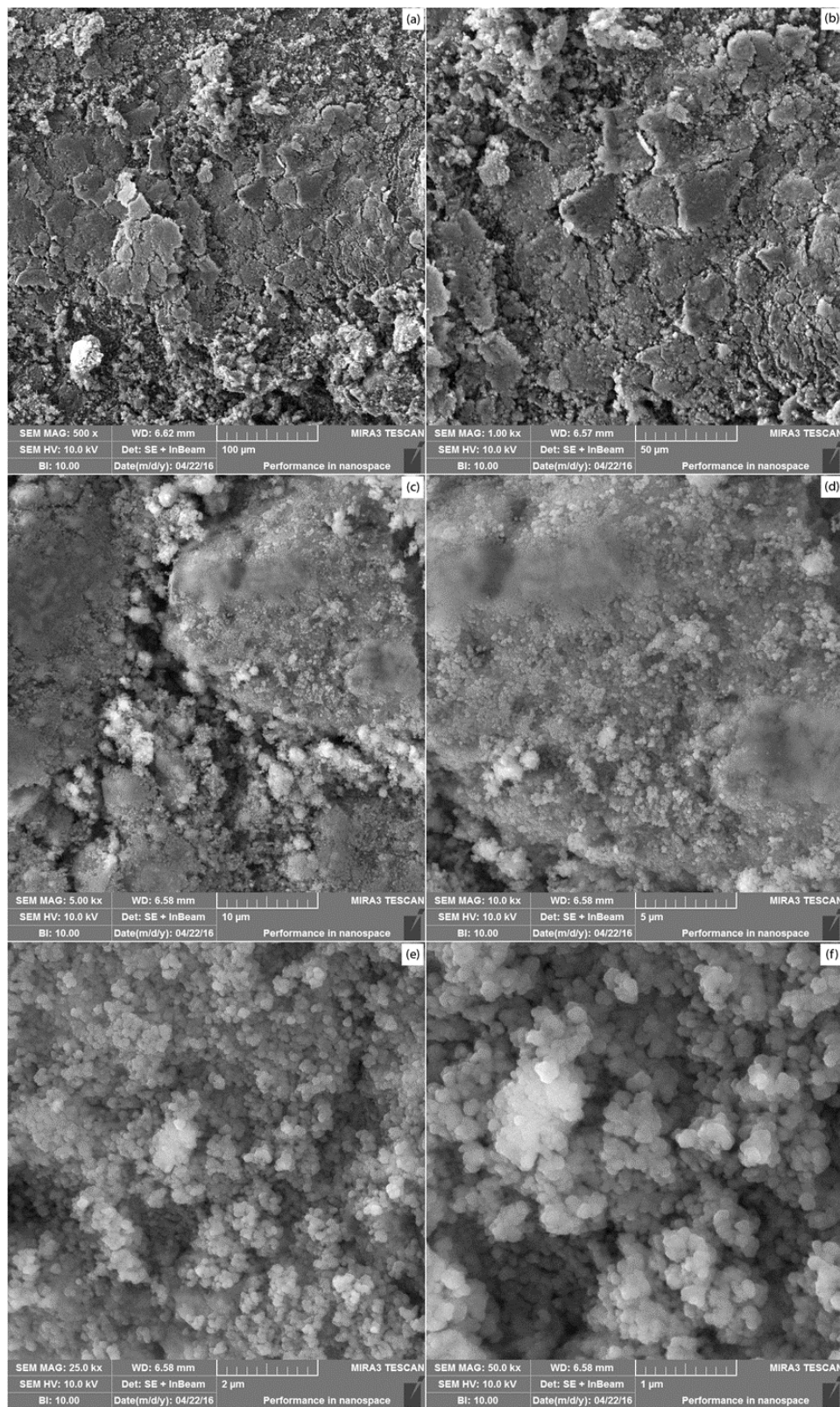
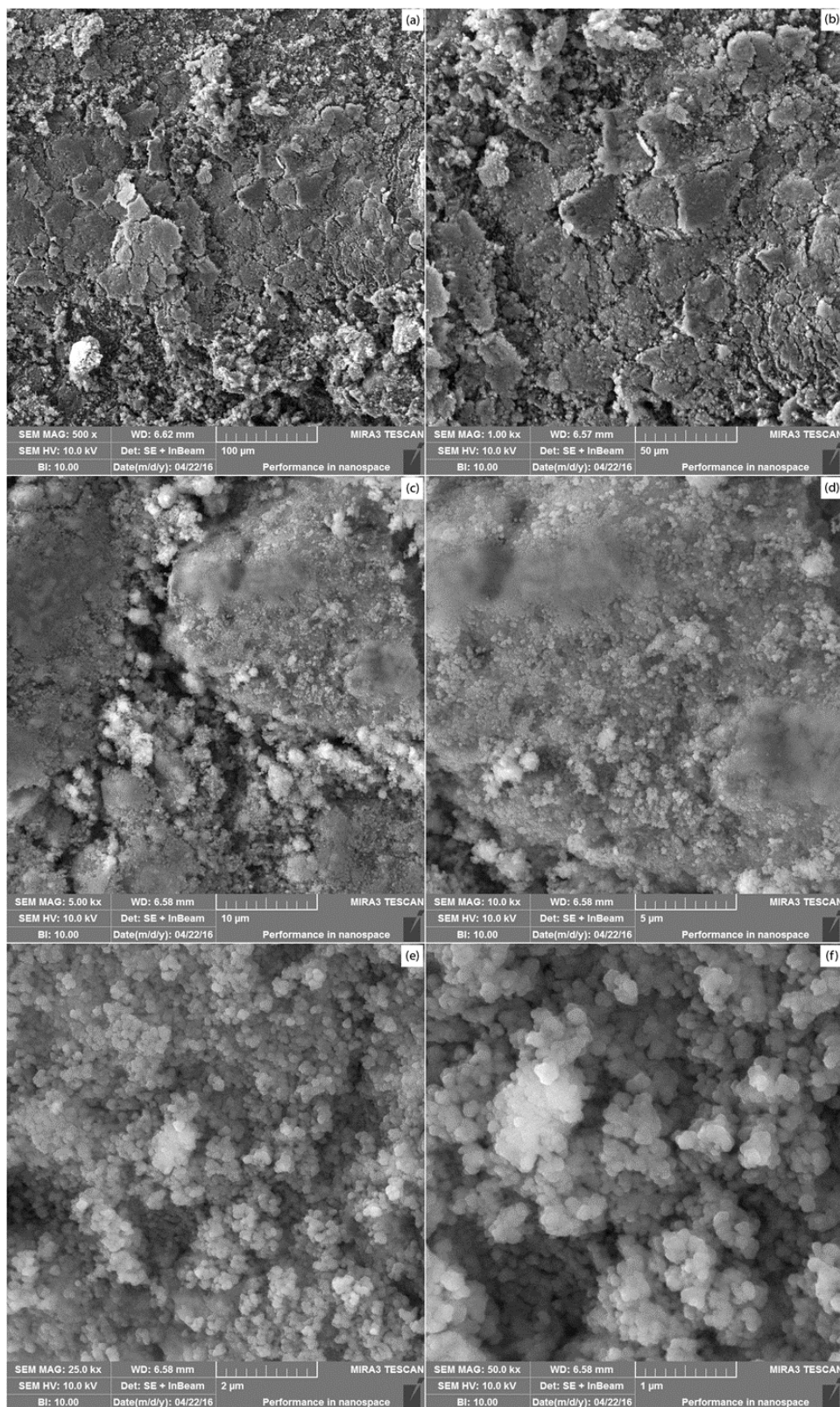


Fig. 2: XRD patterns of zeolite-zeolite (MFI-FAU) Composite Catalyst-A, Catalyst-B, and Catalyst-C, where, Z = ZSM-5 and Y = Y-Zeolite.



**Fig. 3:** SEM image of as-synthesized zeolite-zeolite (MFI-FAU) Composite Catalyst-A.



**Fig. 4:** SEM image of as-synthesized zeolite-zeolite (MFI-FAU) Composite Catalyst-B.

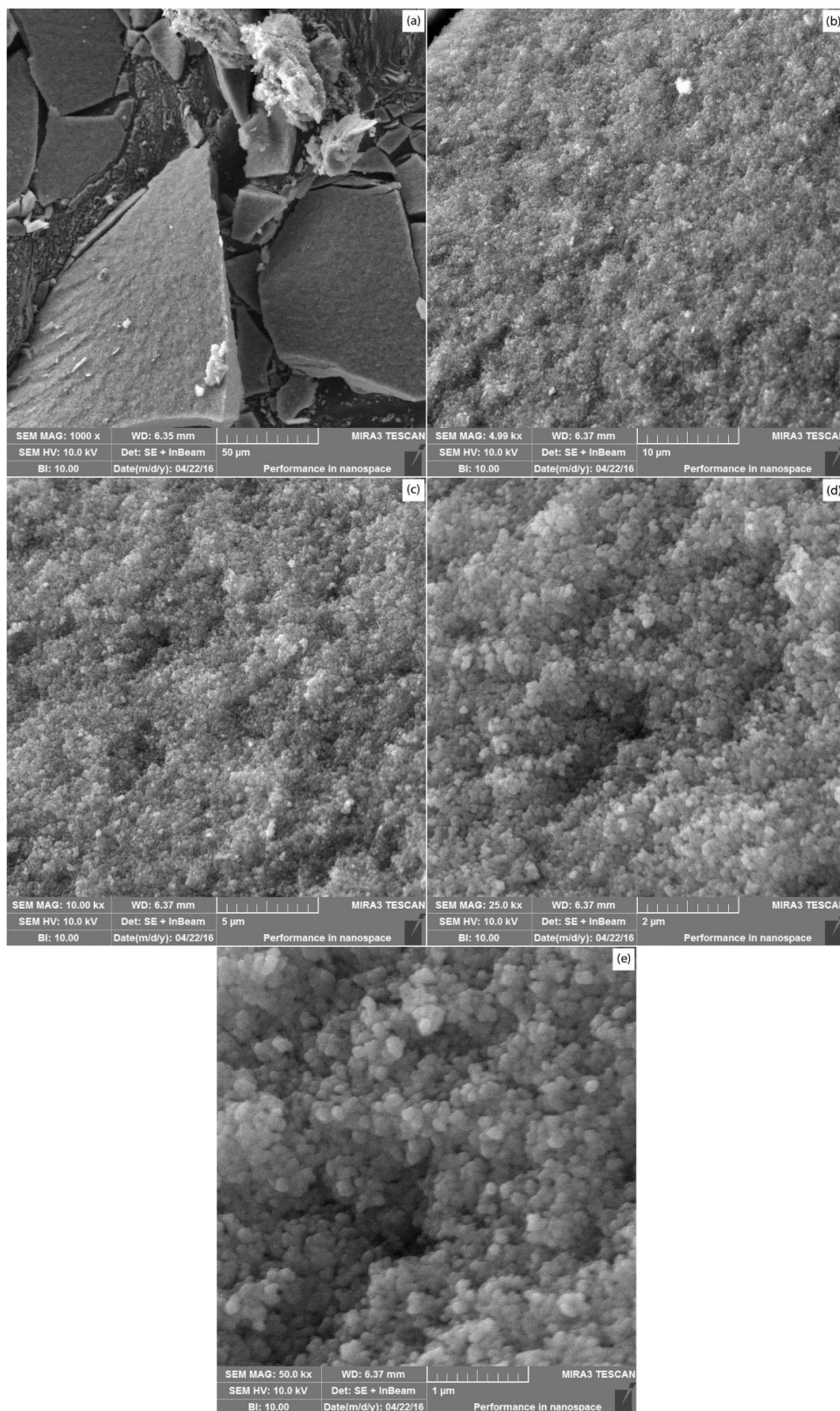


Fig. 5: SEM image of as-synthesized zeolite-zeolite (MFI-FAU) Composite Catalyst-C.

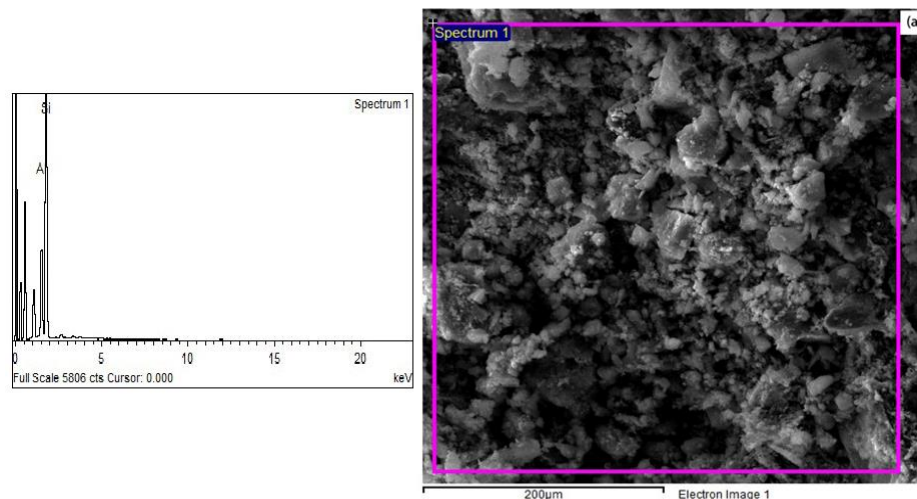


Fig. 6: EDX analysis of as-synthesized zeolite-zeolite (MFI-FAU) Composite Catalyst-A.

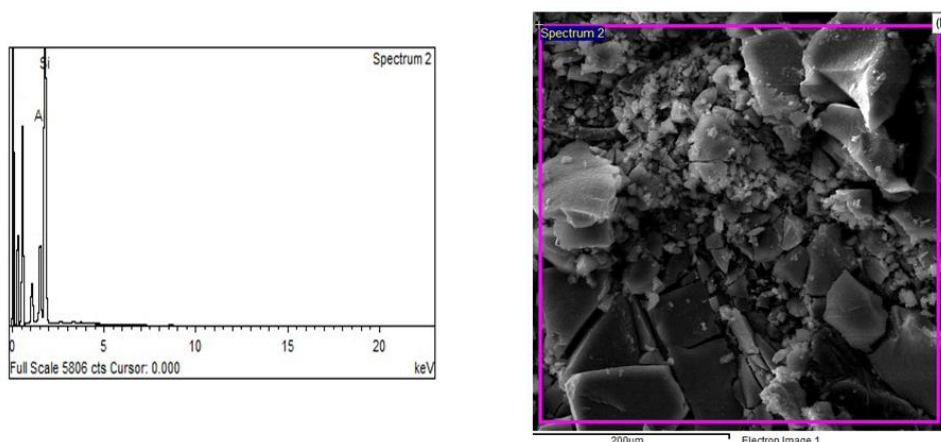


Fig. 7: EDX analysis of as-synthesized zeolite-zeolite (MFI-FAU) Composite Catalyst-B.

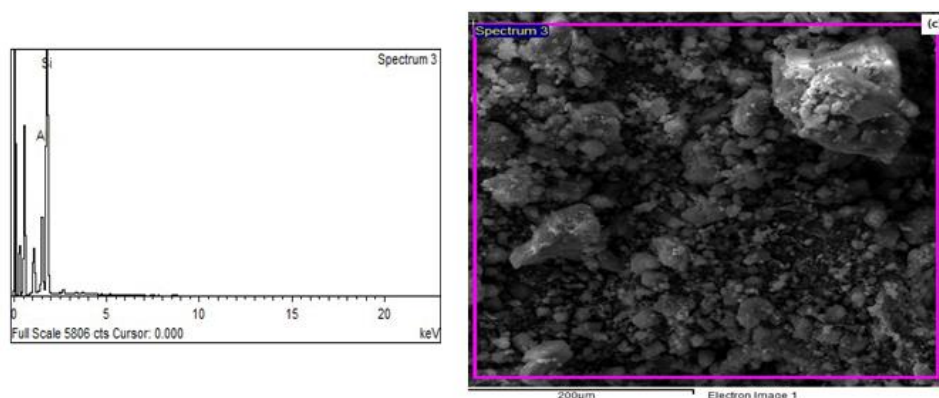


Fig. 8: EDX analysis of as-synthesized zeolite-zeolite (MFI-FAU) Composite Catalyst-C.

It is also understood that the aluminum gradient has significant effect and control on silicon extraction throughout zeolite particles. Silicon extraction from ZSM-5 zeolite takes place in an alkaline solution in the aluminum-poor bulk instead of aluminum-rich

external surface on account of high framework. It is known that high aluminum concentration prevents silicon extraction whereas a low aluminum concentration may result into excessive extraction and formation of hollow zeolite crystals [12, 20, 21].

Fig. 9 represents the FT-IR Spectra of the as-synthesized zeolite-zeolite (MFI-FAU) composite catalysts. The FT-IR spectra of the synthesized zeolite-zeolite (MFI-FAU) composite catalysts were investigated in the infrared band range of 400-4000  $\text{cm}^{-1}$ . It is well noted that infrared band at 484  $\text{cm}^{-1}$  indicates the bending of  $\text{-TO}_4$  (T= Si, Al) tetrahedra of corresponding ZSM-5 structure, while infrared band at 534  $\text{cm}^{-1}$  reflects the tetrahedral vibration of double five-membered ring of pentasil zeolitic material which in turn confirms the presence of ZSM-5 zeolite crystal in synthesized composite catalysts. Furthermore, external linkage symmetrical stretching and internal tetrahedral symmetrical stretching at infrared band of 632  $\text{cm}^{-1}$  and 790  $\text{cm}^{-1}$  and internal tetrahedral asymmetrical stretching and external linkage asymmetrical stretching at infrared band of 1019  $\text{cm}^{-1}$  and 1030  $\text{cm}^{-1}$  of T-O-T (T= Si, Al) of the zeolite framework further strengthen the possibility of the presence of ZSM-5 zeolite crystal in synthesized composite catalysts. The appearance of shoulder peak at 1250  $\text{cm}^{-1}$  indicates the asymmetrical stretching of external framework of MFI-FAU composite catalyst. The adsorbed water molecules showed H-OH bending vibration at around 1651  $\text{cm}^{-1}$  [18, 22-26].

Similarly, infrared band at 460  $\text{cm}^{-1}$  indicates the bending of  $\text{TO}_4$  (T= Si, Al) tetrahedra of corresponding Y-zeolite structure, while infrared band at 576  $\text{cm}^{-1}$  ascribes hexatomic ring vibration of Y-zeolite crystal in synthesized composite catalysts. Furthermore, external linkage symmetrical stretching and internal tetrahedral symmetrical stretching at

infrared band of 680  $\text{cm}^{-1}$  and 713  $\text{cm}^{-1}$  and internal tetrahedral asymmetrical stretching and external linkage asymmetrical stretching at infrared band of 1019  $\text{cm}^{-1}$  and 1024  $\text{cm}^{-1}$  of T-O-T (T= Si, Al) of the zeolite framework further strengthen the presence of Y-zeolite crystal in synthesized composite catalysts [18, 22-26]. It has been seen from the Fig. 9 that hexatomic vibration of Y-zeolite at band 590  $\text{cm}^{-1}$  has been increased vis-à-vis decreased in the pentasil vibration of ZSM-5 zeolite, which reflects that alkalinity of hydrolysis process assisted in the silicon extraction from ZSM-5 framework. The inferences obtained suggest that depolymerization of ZSM-5 framework in basic medium resulted in the formation of zeolite-zeolite composite catalyst. Furthermore, the band of Y-zeolite in as-synthesized composite catalyst shifted from 1018  $\text{cm}^{-1}$  of Catalyst-A, to 1024  $\text{cm}^{-1}$  of Catalyst-B and to 1029  $\text{cm}^{-1}$  of Catalyst-C. The results obtained agree with the EDX results, suggesting that Si/Al ratio of composite catalysts has been decreased as the Y-zeolite ratio increased which is due to the extraction of silicon specie from ZSM-5 framework [27-33].

The aforementioned FT-IR spectra results agree with XRD inferences by clarifying that the transfer of MFI structure into FAU structure is a gradual change process which in turn results in the formation of zeolite-zeolite (MFI-FAU) composite catalysts [12]. The results may differ and shifting of band may occur as the prepared catalysts were composite instead of single zeolitic material such as ZSM-5 or Y-zeolite.

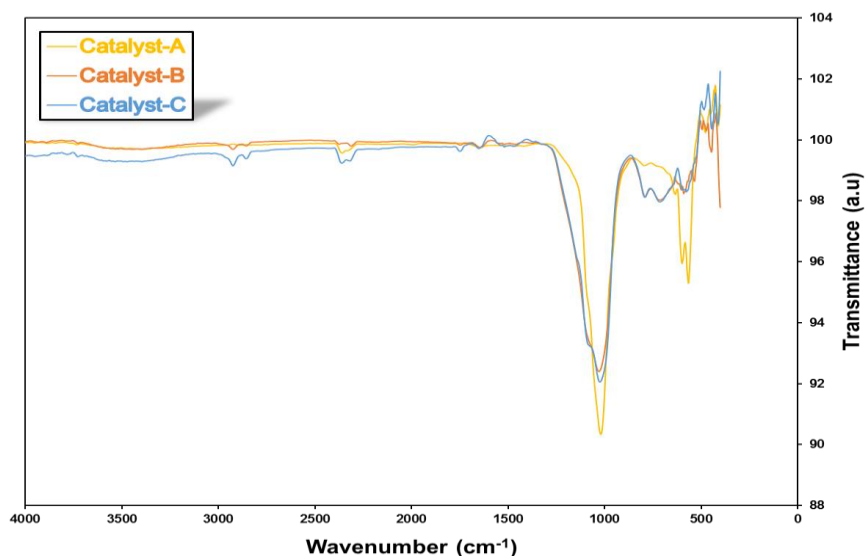


Fig. 9: FT-IR Spectrum of as-synthesized zeolite-zeolite (MFI-FAU) Composite Catalysts.

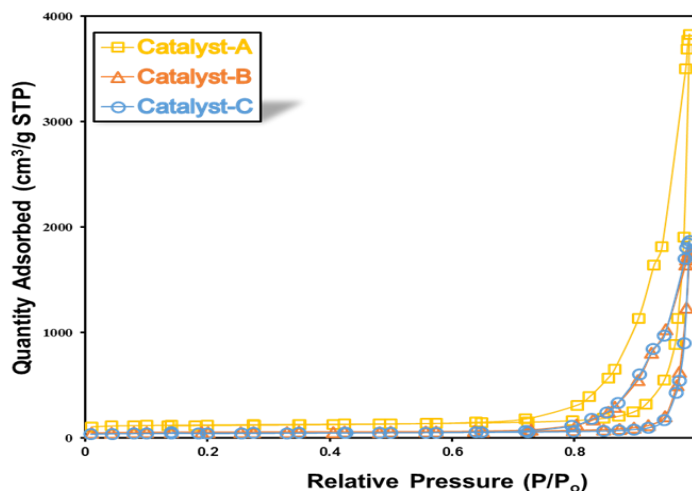


Fig. 10: N<sub>2</sub> adsorption-desorption isotherm of as-synthesized zeolite-zeolite (MFI-FAU) Composite Catalysts.

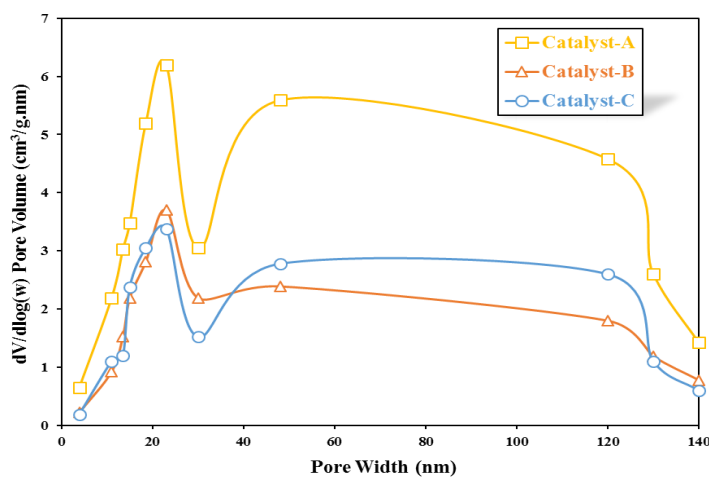


Fig. 10.1: BJH pore size distribution curves of as-synthesized zeolite-zeolite (MFI-FAU) Composite Catalysts.

Fig. 10 represents the N<sub>2</sub> adsorption-desorption on as-synthesized zeolite-zeolite (MFI-FAU) composite catalysts. As can be seen from Fig. 10 that *type-IV* isotherm is observed in zeolite-zeolite (MFI-FAU) composite catalysts, which is a typical feature of mesoporous material. Fig. 10.1 depicts the BJH pore size distribution curves of the as-synthesized zeolite-zeolite (MFI-FAU) composite catalysts, which assures the presence of mesopores with a pore size of about 10 nm in as-synthesized zeolite-zeolite (MFI-FAU) composite catalysts. It was also observed from Fig. 10.1, that pore size of zeolite-zeolite composite catalyst is bimodal [34-36]. The mesoporosity in zeolite-zeolite (MFI-FAU) composite catalysts may occur due to the silicon extraction of ZSM-5 phase by the alkalinity present in synthesis solution and also due to the aggregation of polycrystalline Y-zeolite present in composite catalysts [12].

In continuation, the presence of hysteresis loops is a particular characteristic of *type-IV* isotherm. As regards this case of as-synthesized zeolite-zeolite (MFI-FAU) composite catalysts, H3 hysteresis loop indicating slit-shaped pores was observed which indicates mesoporosity of the material. Moreover, the pronounced uptake of N<sub>2</sub> connected with sharp condensation in the domain of  $P/P_0 \cong 0.8$  confirms the capillary condensation caused by the filling of interparticle spaces in open mesopores [12, 34-36].

The Brunauer, Emmet, and Teller (BET) surface area of Catalyst-A, Catalyst-B, and Catalyst-C was found to be 409.104 m<sup>2</sup>/g, 186.9525 m<sup>2</sup>/g, 151.9215 m<sup>2</sup>/g respectively. The BET surface area, Langmuir surface area, micropore area, micropore volume, external surface area, and pore size distribution are tabulated in Table-4. It was observed that dissolution and partial amorphization of ZSM-5 framework resulted in decreased BET surface area [12].

The catalytic performance of as-synthesized zeolite-zeolite (MFI-FAU) composite catalysts is assessed by isomerizing *n*-hexane. The pictorial representation of composite catalyst in the reaction tube before and after the reaction is depicted in Fig. 11, whereas Fig. 12 represents the images of various as-synthesized zeolite-zeolite (MFI-FAU) composite catalysts before and after the reaction at different temperatures. The difference in color of the composite catalysts sample before and after reaction is mainly due to the formation of carbonaceous products on active sites and cavities of composite catalysts. Fig. 13 depicts the conversion of *n*-hexane with respect to time over Catalyst-A and Catalyst-B at 200 °C, whereas, Fig. 14 represents the conversion of *n*-hexane with respect to time over Catalyst-C at 220°C, 220°C, 240°C, respectively. The catalytic isomerization of *n*-hexane over composite catalysts has been performed for 2.5 h and sampling of isomerization product has been made after every 30 min. Fig. 13 shows that, at 200°C, Catalyst-A and Catalyst-B have reflected conversion of 84% and 67%, respectively. Similarly, Fig. 14 depicts that Catalyst-C has displayed conversion of 88%, 86%, and 90% at 200°C, 220°C, and 240 °C, respectively. In spite of the shorter time provided for reaction, it was noted that all the composite catalysts, i.e., Catalyst-A, Catalyst-B and Catalyst-C presented better and suitable conversions of *n*-hexane over time. The evaluation of catalytic isomerization of composite catalysts indicates that, the mesoporosity introduced in the composite catalysts has significant effect on both diffusion rate and diffusion path of reactant molecules [12]. In catalytic isomerization of *n*-hexane, both Y-zeolite and ZSM-5 zeolite play their individual important role in the form of composite catalysts. The as-synthesized zeolite-zeolite (MFI-FAU) composite catalysts ensured and represented reasonable activity during the catalytic isomerization reaction by providing easy access to acid sites. The catalytic isomerization over composite catalysts as compared to catalytic isomerization over ZSM-5 zeolite is much better due to shortened diffusion distance and diffusion path of reactant molecules and also due to mesoporosity which guarantee the faster diffusion of reactant molecules [12, 19-21]. The as-synthesized zeolite-zeolite (MFI-FAU) composite catalysts guarantee the catalytic isomerization of *n*-hexane by transmitting reactant molecule from relatively large mesopores of Y-zeolite to the relatively small mesopores of ZSM-5 zeolite [12, 37, 38]. The properties of reaction products, i.e. isomers can be finely

improved by tuning ratio of Y-zeolite and ZSM-5 in composite catalysts [12].

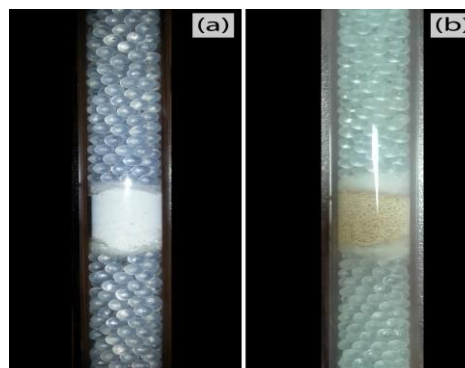


Fig. 11: Pictorial representation of Composite Catalyst in the reaction tube: (a) before the reaction (b) after the reaction.



Fig. 12: Images of: (a) Catalyst-A before the reaction at 200 °C (b) Catalyst-A after the reaction at 200 °C (c) Catalyst-B before the reaction at 200 °C (d) Catalyst-B after the reaction at 200 °C (e) Catalyst-C before the reaction at 200 °C (f) Catalyst-C after the reaction at 200 °C (g) Catalyst-C after the reaction at 220 °C (h) Catalyst-C after the reaction at 240 °C.

Table-4: Textural properties of Zeolite-Zeolite (MFI-FAU) Composite catalysts.

Sample	BET Surface area (m <sup>2</sup> /g)	Langmuir Surface area (m <sup>2</sup> /g)	Micropore Area (m <sup>2</sup> /g)	External Surface Area (m <sup>2</sup> /g)	Pore volume (cm <sup>3</sup> /g)		Mean Pore size (Å)
					Micropore (t-plot)	Total (P/P <sub>0</sub> = 0.964)	
Catalyst-A <sup>†1</sup>	409.104	565.2370	301.2241	107.880	0.146788	1.374885	134.4288
Catalyst-B <sup>†2</sup>	186.9525	258.3766	137.1566	49.7959	0.066827	0.775761	165.9803
Catalyst-C <sup>†3</sup>	151.9215	210.2891	100.1889	51.7326	0.048805	0.669164	176.1868

Catalyst-A<sup>†1</sup> = ZSM-5 + 2 g Y-Zeolite, Catalyst-B<sup>†2</sup> = ZSM-5 + 3 g Y-Zeolite Catalyst-C<sup>†3</sup> = ZSM-5 + 4 g Y-Zeolite

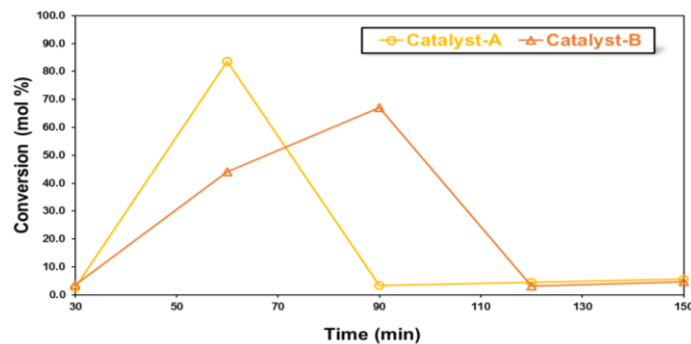


Fig.13: Conversion of *n*-hexane over Catalyst-A and Catalyst-B. Reaction condition:  $T = 200\text{ }^{\circ}\text{C}$ ,  $\text{WHSV} = 0.06\text{ g. h}^{-1}/\text{g-catalyst}$ , atmospheric pressure.

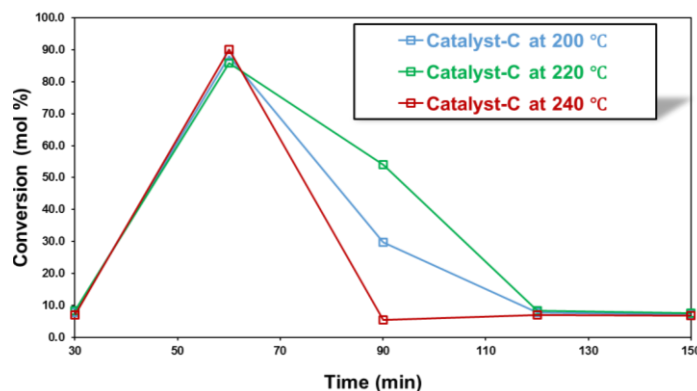


Fig. 14: Conversion of *n*-hexane over Catalyst-C at different Temperatures. Reaction condition:  $\text{WHSV} = 0.25\text{ g. h}^{-1}/\text{g-catalyst}$ , atmospheric pressure.

Acidity of composite catalysts were not measured directly, however, the increased activity of the Catalyst-C shows that it has highest acidity as isomerization reaction requires acidic sites, because, the acidic sites of the zeolites assists in carbo-cation isomerization reaction. It has been observed from EDX analysis that Si/Al ratio of composite catalysts has been decreased as the amount of Y-zeolite in the composite catalyst increase. In addition, the spectra of as-synthesized composite catalysts indicate the presence of Lewis acid sites at band  $2330\text{-}2360\text{ cm}^{-1}$  and Bronsted acid sites at band  $1643\text{-}1651\text{ cm}^{-1}$ . The strength of Bronsted acid sites follows an order of Catalyst-C > Catalyst-B > Catalyst-A. Comparatively, high Bronsted/Lewis are because of multiple reasons, including, alkalinity of hydrolysis process, destruction of Si-O-Si and Si-O-Al bonds in ZSM-5 framework, amorphization of ZSM-5, as well as formation of additional AlOH groups in the composite catalysts. The unique crystalline nature of composite catalysts plays role in isomerization reaction as mesoporous promotes faster diffusion of reactant/product molecule to active centers, better accessibility to guest molecules to Bronsted active sites and also assists in faster mass and heat transfer mechanisms. In this work, it was noted that density and strength of Bronsted acid sites have significant

effect on isomerization reaction mechanism. Catalyst-C with stronger Bronsted acid sites displayed highest conversion at  $240^{\circ}\text{C}$  but also resulted in faster deactivation due to site coverage and pore blockage by coke deposits. This type of behavior is expected for zeolitic catalysts, as hydrogen is not present in the feed, therefore, more active zeolite catalyst gives more coke formation and quick deactivation. In case of Catalyst-C, we can observe that at higher temperature, *i.e.*,  $240^{\circ}\text{C}$ , deactivation occurs quickly to reach the stable state of the catalyst. Initially, activity of all the composite catalysts increased linearly with acidity, however, decreases subsequently due to rapid deactivation of catalysts having highest no. of acid sites [13-15, 39, 40].

## Conclusions

A number of zeolite-zeolite (MFI-FAU) composite catalysts are synthesized by incorporating previous practices and techniques. The chemical and physical features of zeolite-zeolite (MFI-FAU) composite catalysts are examined and characterized by using powder X-ray diffraction (XRD), scanning electron microscopy (SEM) coupled with energy-dispersive X-ray spectrometry (EDX),  $\text{N}_2$  adsorption-desorption measurements (BET, BJH, t-plot

measurements) and Fourier transform infrared (FTIR) spectroscopy equipped with attenuated total reflectance (ATR) arrangements. The characterization inferences confirm the following salient observations in the as-synthesized zeolite-zeolite (MFI-FAU) composite catalysts:

- The presence of ZSM-5 and Y-zeolite phase in the as-synthesized zeolite-zeolite (MFI-FAU) composite catalysts by the SEM-EDX results.
- The XRD patterns depict the crystalline nature of as-synthesized zeolite-zeolite (MFI-FAU) composite catalysts by observing the well-defined distinct peaks of ZSM-5 and Y-zeolite.
- The FT-IR spectra obtained show the significant infrared band of ZSM-5 and Y-zeolite in the as-synthesized zeolite-zeolite (MFI-FAU) composite catalysts.
- The BET results suggest mesoporosity in the as-synthesized zeolite-zeolite (MFI-FAU) composite catalysts with a pore size of 10-15 nm.

Keeping in view the above facts, the aim is to produce relatively novel zeolite-zeolite (MFI-FAU) composite catalysts having potential of catalyzing isomerization of lighter hydrocarbon, *i.e.*, *n*-hexane with better efficiency. It is well noted that the maximum conversion of 90% is displayed by Catalyst-C at 240°C.

#### Acknowledgement

We greatly acknowledge Ms Dureem and Muhammad Sarfraz Akram for their kind support in the completion of this project.

#### References

1. A. Clements, M. Dunn, V. Firth, L. Hubbard, J. Lazonby, D. Waddington, The Essential Chemical Industry [online] Chemical Industry Education Centre: University of York, UK, 2010. <http://www.essentialchemicalindustry.org/processes/cracking-isomerisation-and-reforming.html> (accessed Jun 30, 2016).
2. P. M. Lima, T. Garetto, Jr. C. L. Cavalcante and D. Cardoso, Isomerization of *n*-hexane on Pt–Ni catalysts supported on nanocrystalline H-BEA zeolite, *Catal. Today*, **172**, 195 (2011).
3. M. R. Usman and F. M. Alotaibi, *Prog. React. Kinet. Mech.*, **41**, 177 (2016).
4. N. Rahimi and R. Karimzadeh, Catalytic cracking of hydrocarbons over modified ZSM-5 zeolites to produce light olefins: A review, *Appl. Catal., A*, **398**, 1 (2011).
5. G. Wang, Y. Liu, J. Zheng, M. Pan, H. Zhang, B. Li, S. Yaun, Y. Yi, H. Tian and R. Li, Zeolite-zeolite composite fabricated by polycrystalline Y zeolite crystals parasitizing ZSM-5 zeolite, *J. Mater. Res.*, **30**, 2434 (2015).
6. H. Teng, J. Wang, D.M. Chen, P. Liu and X.C. Wang, Silicalite-1 membrane on millimeter-sized HZSM-5 zeolite extrudates: Controllable synthesis and catalytic behavior in toluene disproportionation, *J. Membr. Sci.*, **381**, 197 (2011).
7. L.X. Jia, X.Y. Sun, X.Q. Ye, C.L. Zou, H.F. Gu, Y. Huang, G.X. Niu and D.Y. Zhao, Core-shell composites of USY@Mesosilica: Synthesis and application in cracking heavy molecules with high liquid yield, *Microporous Mesoporous Mater.*, **176**, 16 (2013).
8. J.Q. Zhang, W.B. Fan, Y.Y. Liu and R.F. Li, Synthesis and catalytic property of a Co 2<sup>+</sup>-exchanged Beta/Y composite for the selective catalytic reduction of NO by CH<sub>4</sub> in the presence of excess oxygen, *Appl. Catal., B*, **76**, 174 (2007).
9. B. Bouizi, K. Haas-Santo, M. Hunger and J. Weitkamp, Synthesis and characterization of aluminum-rich zeolite ZSM-5, *Chem. Eng. Technol.*, **23**, 322 (2000).
10. M. Yee and I.I. Yaacob, Synthesis and characterization of iron oxide nanostructured particles in Na–Y zeolite matrix, *J. Mater. Res.*, **19**, 930 (2004).
11. S. Soltanali, R. Holladj, A. Rashidi, M. Bazmi and F. Bahadoran, The effect of HZSM-5 catalyst particle size on kinetic models of methanol to gasoline conversion, *Chem. Eng. Res. Des.*, **106**, 33 (2016).
12. B. Ren, S.Y. Bai, J.H. Sun, F.Q. Zhang, and M.H. Fan, Controllable synthesis of obvious core-shell structured Y/beta composite zeolite by a stepwise-induced method, *RSC Adv.*, **4**, 22755 (2014).
13. Q. Zhao, B. Qin, J. Zheng, Y. Du, W. Sun, F. Ling and R. Li, Core-shell structured zeolite-zeolite composites comprising Y zeolite cores and nano-β zeolite shells: Synthesis and application in hydrocracking of VGO oil, *Chem. Eng. J.*, **257**, 262 (2014).
14. A. S. Kovo, E. Opuama, M. O. Edoga, M. Abdulkadir, A. G. Isah and I. A. Mohammed, On the Synthesis of Zeolite Y/ZSM-5 Composite via Novel Technique, *Chem. Eng. Sci.*, **4**, 1 (2016).
15. S. Al-Khattaf, A. Iliyas, A. Al-Amer and T. Inui, The effect of Y-zeolite acidity on *m*-xylene transformation reactions, *J. Mol. Catal. A: Chem.*, **225**, 117 (2005).
16. M.M. Treacy and J.B. Higgins, Collection of simulated XRD powder patterns for zeolites, 5th ed., Elsevier, (2007).
17. F. Jin, Y. Cui, Z. Rui and Y. Li, Effect of sequential desilication and dealumination on

- catalytic performance of ZSM-5 catalyst for pyridine and 3-picoline synthesis, *J. Mater. Res.*, **25**, 272 (2010).
18. Y. Li, H. Sun, R. Feng, Y. Wang, F. Subhan, Z. Yan, Z. Zhang and Z. Liu, Synthesis of ZSM-5 zeolite from diatomite for fluid catalytic cracking (FCC) application, *Appl. Petrochem. Res.*, **5**, 347 (2015).
  19. J.J. Zheng, Q.H. Zeng, Y.Y. Zhang, Y. Wang, J.H. Ma, X.W. Zhang, W.F. Sun and R.F. Li, Hierarchical Porous Zeolite Composite with a Core-Shell Structure Fabricated Using  $\beta$ -Zeolite Crystals as Nutrients as Well as Cores, *Chem. Mater.*, **22**, 6065 (2010).
  20. J.C. Groen, W. Zhu, S. Brouwer, S.J. Huynink, F. Kapteijn, J.A. Moulijn and J. Pérez-Ramírez, Direct demonstration of enhanced diffusion in mesoporous ZSM-5 zeolite obtained via controlled desilication, *J. Am. Chem. Soc.*, **129**, 355 (2007).
  21. J. C. Groen, T. Bach, U. Ziese, A. M. Paulaimevan Donk, K. P. de Jong, J. A. Moulijn and J. Pérez-Ramírez, Creation of hollow zeolite architectures by controlled desilication of Al-zoned ZSM-5 crystals, *J. Am. Chem. Soc.*, **127**, 10792 (2005).
  22. I. R. Shaikh, R. A. Shaikh, A. A. Shaikh, J. A. War, S. P. Hangirgekar, A. L. Shaikh, P.R. Shaikh and R. R. Shaikh, H-ZSM-5 zeolite synthesis by sourcing silica from the wheat husk ash: characterization and application as a versatile heterogeneous catalyst in organic transformations including some multicomponent reactions, *J. Catal.*, 2015.
  23. Q. Tang, H. Xu, Y. Zheng, J. Wang, H. Li, & J. Zhang, Catalytic dehydration of methanol to dimethyl ether over micro-mesoporous ZSM-5/MCM-41 composite molecular sieves, *Appl. Catal., A*, **413**, 36 (2012).
  24. Y. Wang, R. Feng, X. Li and Z. Yan, In situ synthesis, characterization and catalytic activity of ZSM-5 zeolites on kaolin microspheres from amine-free system, *J. Porous Mater.*, **20**, 137 (2013).
  25. S. Sengupta, D. Ghosal, J. K. Basu and P. Kamble, Chemical modification of HZSM-5 for selective methylation, *Int. J. Chem. React. Eng.*, **10**, 2012.
  26. M. Asadollahi, D. Bastani and H. Kazemian, Permeation of single gases through TEG liquid membranes modified by Na-Y nano-zeolite particles, *Sep. Purif. Technol.*, **76**, 120 (2010).
  27. Z. Tvaruzkova and V. Bosacek, Characterization of hydroxyl groups of Y zeolites by infrared spectra, *Chem. zvesti*, **29**, 325 (1975).
  28. J. Zheng, Q. Zeng, Y. Yi, Y. Wang, J. Ma, B. Qin and R. Li, The hierarchical effects of zeolite composites in catalysis, *Catal. Today*, **168**, 124 (2011).
  29. J. Weitkamp, Zeolites and Catalysis, *Solid State Ionics*, **131**, 175 (2000).
  30. E. Escalona Platero, M. Penarroya Mentrut and C. Morterra, Fourier Transform Infrared Spectroscopy Study of CD<sub>3</sub>CN Adsorbed on Pure and Doped  $\gamma$ -Alumina, *Langmuir*, **15**, 5079 (1999).
  31. R.C. Deka, Acidity in zeolites and their characterization by different spectroscopic methods, *Indian J. Chem. Technol.*, **5**, 109 (1998).
  32. G. Li, Ph.D. Thesis, *FT-IR studies of zeolite materials: characterization and environmental applications*, University of Iowa, (2005).
  33. W. Mozgawa, M. Król and K. Barczyk, FT-IR studies of zeolites from different structural groups, *Chemik*, **65**, 667 (2011).
  34. D. A. de Haro-Del Rio, A. F. Aguilera-Alvarado, I. Cano-Aguilera, M. Martínez-Rosales and S. Holmes, Synthesis and characterisation of mesoporous aluminosilicates for copper removal from aqueous medium, *Mater. Sci. Appl.*, **3**, 485 (2012).
  35. W. Fan, M. A. Snyder, S. Kumar, P. S. Lee, W. C. Yoo, A. V. McCormick and M. Tsapatsis, Hierarchical nanofabrication of microporous crystals with ordered mesoporosity, *Nat. Mater.*, **7**, 984 (2008).
  36. K.S.W. Sing, D.H. Everett, R.A.W. Haul, L. Moscou, R.A. Pierotti, J. Rouquero and T. Siemieniowska, Reporting physisorption data for gas/solid systems — with special reference to the determination of surface area and porosity, *Pure Appl. Chem.*, **57**, 603 (1985).
  37. K. Na and G.A. Somorjai, Hierarchically nanoporous zeolites and their heterogeneous catalysis: current status and future perspectives, *Catal. Lett.*, **145**, 193 (2015).
  38. X.Y. Yang, G. Tian, L.H. Chen, Y. Li, J.C. Liu, Z. Deng, G. Van Tendeloo and B.L. Su, Well-Organized Zeolite Nanocrystal Aggregates with Interconnected Hierarchically Micro-Meso-Macropore Systems Showing Enhanced Catalytic Performance, *Chem. - Eur. J.*, **17**, 14987 (2011).
  39. S. Al-Khattaf, A. Iliyas, A. Al-Amer and T. Inui, The Effect of Y-zeolite Acidity on m-Xylene Transformation Reactions, *J. Mol. Catal. A: Chem.*, **225**, 117 (2005).
  40. S. Van Donk, J. H. Bitter and K. P. De Jong, Deactivation of solid acid catalysts for butene skeletal isomerisation: on the beneficial and harmful effects of carbonaceous deposits, *Appl. Catal., A*, **212**, 97 (2001).